On the Hot Corrosion of Nickel at 700 °C

Thomas Gheno, Brian Gleeson

On the hot corrosion of nickel at 700 °C

Thomas Gheno and Brian Gleeson
Department of Mechanical Engineering and Materials Science,
University of Pittsburgh, Pittsburgh PA 15261, USA
Email: thg14 at pitt.edu; bgleeson at pitt.edu

This is a post-peer-review, pre-copyedit version of an article published in Oxidation of Metals. The final version is available online at:
https://doi.org/10.1007/s11085-015-9588-6

Abstract The reaction of nickel with Na_2SO_4 was studied in an O_2–$0.1SO_2$ atmosphere at 700 °C, conditions typical of type II hot corrosion. The interaction of NiO with the sulfate was thermodynamically analyzed and compared with the dissolution–precipitation process known to occur at higher temperatures. Here the dissolution stage was short-lived due to a positive solubility gradient for Ni^{2+}. The relatively fast growth of a NiO layer above a nickel sulfide layer was attributed to the inward molecular transport of SO_2–SO_3 through the porous NiO. The influence of environmental variables was further assessed by reacting nickel with and without Na_2SO_4 in air and then with no deposit in O_2–$0.1SO_2$. The roles of the deposit and atmosphere on the boundary conditions affecting the oxidation–sulfidation process were discussed on the basis of the observed reaction paths.

Keywords Nickel; Sodium sulfate; Hot corrosion; Sulfidation

1 Introduction

Hot corrosion of high-temperature materials involves the growth of an oxide scale on the metal surface, its dissolution into a molten sulfate (the reactivity of which depends on its interaction with the gas phase), and the formation of sulfides which can also be liquid. Given this mechanistic complexity, pure metals prove particularly useful in the study of hot corrosion, and provide a framework to analyze the yet more complex behavior of alloys and commercial materials. Nickel is of particular interest since it forms the base of many high-temperature materials.

The reaction of nickel with Na_2SO_4 as the prototypical sulfate deposit has mostly been documented in type I conditions, i.e., at temperatures above the Na_2SO_4 melting point (T_m = 884 °C). The accelerated corrosion may be associated with basic fluxing of NiO [1–4]. Briefly, as NiO growth consumes oxygen and oxygen transport in the melt is slow, a p_{O_2} gradient is established which results in elevated sulfur activities at the oxide/sulfate interface by virtue of the following equilibrium:

$$SO_3 = \frac{1}{2}S_2 + \frac{3}{2}O_2 \tag{1}$$

This can then lead to sulfidation if the oxide is permeable to sulfur-bearing molecules. The simultaneous removal of sulfur and oxygen from the melt at the oxide surface results in a local decrease in p_{SO_3}, which prompts the basic dissolution of NiO via nickelate ion formation, NiO_2^{2-}. Away from the scale, the p_{SO_3} is higher, and so is the solubility of nickelate ions: this "negative solubility gradient" causes NiO to precipitate within the sulfate as a non-protective scale.

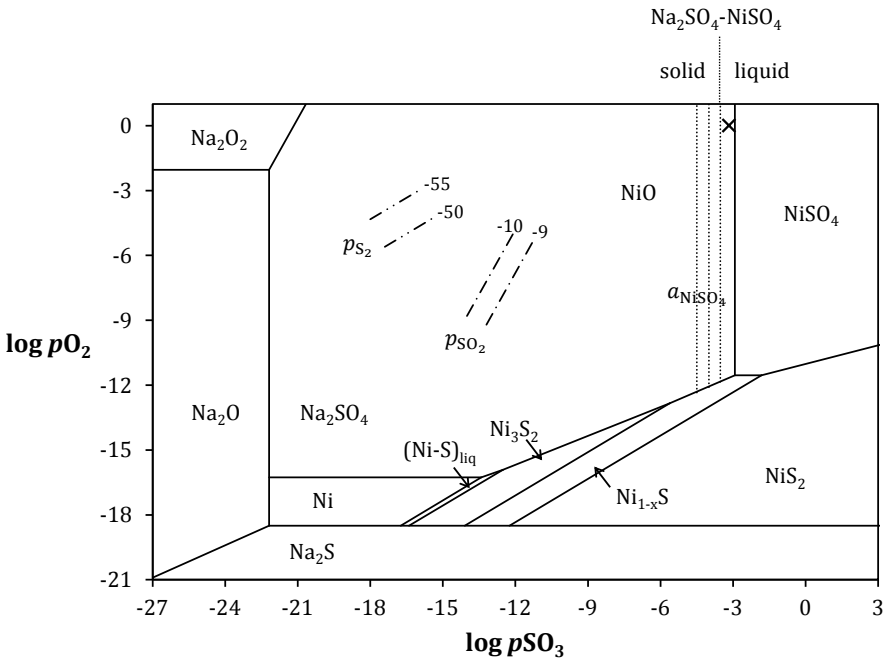

Figure 1: Superimposed stability diagrams of Ni–O–S and Na–O–S systems at 700 °C, plotted with $\log p_{SO_3} - \log p_{O_2}$ coordinates from data in Refs. [7,8], making the assumption of unit activity for all compounds. The mixed compounds Na_2NiO_2 and $NaNiO_2$ are missing by lack of reliable data. Iso-p_{S_2}, iso-p_{SO_2} and iso-a_{NiSO_4} directions are indicated with dashed lines (values of $\log p_{S_2}$ and $\log p_{SO_2}$ are indicated). The p_{SO_3} at equilibrium between solid and liquid Na_2SO_4–$NiSO_4$ solutions is from Misra et al. [9]. The cross marks the equilibrium composition of a gas mixture of initial composition O_2–0.1SO_2 at 700 °C.

Low temperature, or type II hot corrosion, which occurs below the melting point of the applied salt, involves the acidification of the salt by an SO_3-containing gas, and reaction of the metal oxide to produce a liquid sulfate solution [5]. This process of gas-phase-induced acidic fluxing [6] is very sensitive to the gas composition, and potentially leads to very high corrosion rates above the eutectic temperature (e.g., T_e (Na_2SO_4–$NiSO_4$) = 671 °C). The thermodynamic aspects of the oxide–sulfate–gas interactions are conveniently represented using stability diagrams. Four species may be present in gases containing oxygen and sulfur at high temperatures (O_2, S_2, SO_2, SO_3), but any composition can be described using two independent partial pressures. Following Goebel and Pettit [1], p_{SO_3} and p_{O_2} were chosen to plot the Ni–O–S diagram at 700 °C in Fig. 1, where the activity of all compounds is taken as unity. The Na–O–S diagram is superimposed. The acidic reaction of NiO is given by

$$NiO + SO_3 = NiSO_4 \tag{2}$$

and is represented by a vertical line (p_{SO_3} = constant). This p_{SO_3} value defines whether a sulfate is considered acidic or basic, relative to NiO. The activities of SO_3 and Na_2O are related through the sulfate dissociation equilibrium

$$Na_2SO_4 = Na_2O + SO_3 \tag{3}$$

Nickel sulfate is soluble in solid and liquid Na_2SO_4 [10]; thus, as the nickel concentration in solid Na_2SO_4 reaches the solidus, and inasmuch as the $NiSO_4$ activity is less than one, a liquid is formed at a lower p_{SO_3} than that required to stabilize pure $NiSO_4$ (s). The thermodynamic interaction was studied in detail in Refs. [5,9], and is illustrated in Fig. 1: the dotted vertical line represents the p_{SO_3} at equilibrium between NiO (s) and solid and liquid Na_2SO_4–$NiSO_4$ solutions estimated by Misra et al. [9]. Alternatively, the acidic dissolution reaction may be written

$$NiO = \underline{Ni^{2+}} + \underline{O^{2-}} \tag{4}$$

(solutes are underlined). A relation between the activity of oxide ions and the p_{SO_3} is obtained by considering the equilibrium

$$SO_4^{2-} = O^{2-} + SO_3 \tag{5}$$

which is equivalent to Eq. (3).

Reaction mechanisms governing type II hot corrosion are less well understood than those of type I. Luthra [11,12] proposed a model for cobalt and Co-base alloys based on a Co^{2+}–Co^{3+} exchange mechanism, which does not apply to nickel. Most of the work on nickel has focused on gas atmospheres with high SO_2–SO_3 contents, i.e., much higher than what would be found in a gas turbine, for example. In particular, Lillerud and Kofstad [13] reported a thorough study conducted in O_2–4 % (SO_2–SO_3) at different pressures at 700 °C, where Ni_3S_2 formed within the NiO scale, and fast nickel diffusion in the sulfide caused high reaction rates. The outward diffusing nickel was then described to react with $NiSO_4$ in the liquid sulfate solution to form NiO and Ni_3S_2.

Since hot corrosion involves sulfidation, its study can benefit to some extent from the abundant literature which exists in the field of gaseous oxidation–sulfidation (see Refs. [14–16] for reviews of the reaction of pure metals). Those previous studies mostly concern SO_2 or O_2–SO_2 mixtures with high SO_2/O_2 ratios. The reaction of nickel in such environments produces intermixed NiO–Ni_3S_2 scales, where the sulfide phase has been shown by resistivity measurements [17] to form a continuous network. Scaling rates vary depending on the phase volume fractions, but can be as much as 10^7 times higher than the oxidation rate at a given temperature [17]. Reaction kinetics are controlled by outward Ni diffusion in the Ni_3S_2 channels, and indeed Ni_3S_2 growth rates are about 10^7 times higher than those of NiO (compare data in Refs. [18,19]). Luthra and Worrell [20] and Giggins and Pettit [21] published detailed studies of the effect of gas composition on the constitution and growth rates of the reaction products. Some variability exists between those results, which is hardly avoidable given the sensitivity of the reaction processes to local conditions.

This paper presents a study of the corrosion of pure nickel coated with Na_2SO_4 in an oxygen-rich, O_2–0.1 % (SO_2–SO_3) gas mixture at 700 °C. Results are also reported of nickel reaction with Na_2SO_4 in air, and with no deposit in O_2–0.1 % (SO_2–SO_3), all other experimental parameters being unchanged. This allowed for a systematic investigation of the role of gas and sulfate chemistry on the reaction mechanism. This work is part of a broader study of type II hot corrosion aiming to better understand the effects of alloying additions in nickel-base alloys, aspects of which have been published elsewhere [22].

2 Experimental procedures

High purity (99.999 %) nickel specimens were cut from a 1 mm thick rolled plate received from Goodfellow. Specimens of dimensions 8 × 8 mm^2 were ground to a P1200 grit finish using SiC paper, then degreased with detergent and ultrasonically cleaned in ethanol before exposure. Isothermal corrosion experiments were conducted at 700 °C using a horizontal tube furnace with flowing O_2–0.1 % SO_2. Linear gas flow rates were about 1 mm s^{-1} at reaction temperature, with a total pressure slightly over 1 atm. The gas was passed through a platinized honeycomb catalyst located directly upstream of the specimens in the hot zone, allowing the otherwise sluggish reaction

$$SO_2 + \frac{1}{2}O_2 = SO_3 \tag{6}$$

to proceed, with an equilibrium p_{SO_3} calculated to be 7.1×10^{-4} atm at 700 °C from data in Ref. [7]. The resulting O_2–SO_2–SO_3 gas mixture will simply be referred to as O_2–0.1SO_2. Sodium sulfate was applied by spraying a saturated aqueous solution on the top surface of a preheated specimen. This produced an approximately uniform 2.8 ± 0.5 mg cm^{-2} Na_2SO_4 deposit.

After exposure, the corrosion products were studied by XRD using a Panalytical Empyrean instrument, with a Co radiation ($K_{\alpha 1}$ = 1.789 Å). Polished sections were then prepared by standard metallographic procedures, using water-free cutting fluid and polishing suspensions to retain water-soluble products (i.e., sodium and nickel sulfates). The cross-sections were characterized by SEM with a JEOL JSM 6510 instrument, and by electron probe micro-analysis (EPMA) using a JEOL JXA 8530F instrument.

The solubility of nickel in Na_2SO_4 is a function of the p_{SO_3}, which can be set through equilibrium with the gas environment. On the basis of a regular solution model for the molten sulfate, Misra et al. [9] determined the Gibbs free energy of the sulfation reaction

$$NiO(s) + SO_3(g) = \underline{NiSO_4}(l) \tag{7}$$

where the underscore denotes solution in Na_2SO_4. They then calculated the minimum p_{SO_3} required for the reaction to proceed, i.e., for the solubility of $NiSO_4$ in solid Na_2SO_4 to be exceeded, and the liquid sulfate to be formed. That minimum p_{SO_3}, 3×10^{-4} atm at 700 °C, is shown in Fig. 1 by the Na_2SO_4–$NiSO_4$ vertical line. The equilibrium gas p_{SO_3} in the present work is seen by the cross in Fig. 1 to be sufficiently high for liquid Na_2SO_4–$NiSO_4$ formation, but lower than that required for solid $NiSO_4$ to be stable. The reaction of Ni with Na_2SO_4 in this gas is thus expected to produce a liquid Na_2SO_4–$NiSO_4$ solution in equilibrium with NiO.

Figure 2 shows the cross-section of a nickel specimen coated with Na_2SO_4 and exposed to O_2–0.1SO_2 for 6.5 h at 700 °C. The reaction products will be described in detail in Section 3; we simply note here that the hot corrosion process was visibly not limited to the surface where Na_2SO_4 was applied, but also extended to the side and bottom faces. The oxide formed on the bottom face near the specimen edge is infiltrated with a Na_2SO_4–$NiSO_4$ mixture (see insert in Fig. 2), which indicates that a liquid sulfate had indeed formed and flowed along the specimen surface. Qualitatively, the formation of a liquid confirms the validity of the system's description based on thermodynamic equilibrium in the gas and the sulfate.

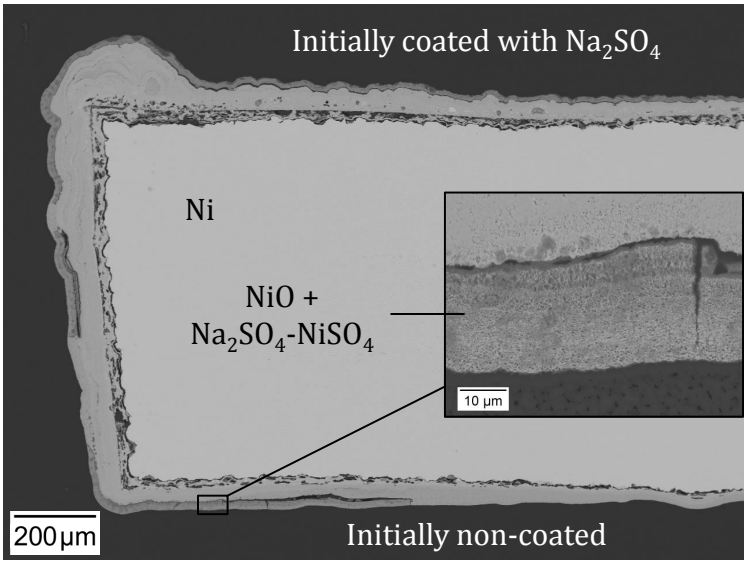

Figure 2: Cross-section of nickel specimen after 6.5 h reaction with Na_2SO_4 in O_2–0.1SO_2 at 700 °C. The oxide scale on the bottom face (i.e., the side which was not coated with Na_2SO_4 prior to exposure) is infiltrated with Na_2SO_4–$NiSO_4$, which indicates that the sulfate mixture was liquid at temperature.

3 Results

The corrosion of nickel beneath a Na_2SO_4 deposit in O_2–0.1SO_2 at 700 °C was studied based on 0.5, 6.5 and 20 h exposures. Analysis by XRD (Fig. 3) showed that the reaction products were NiO and Ni_3S_2 in all cases. Scale thicknesses varied significantly between the center and the edges of the specimens. For example, after 6.5 h, the scale was found to be on average 40 µm thick in the center, and to exceed 200 µm on the edges (see Fig. 2). This discrepancy prevented global measurement methods such as thermogravimetry to provide reliable results. The abnormally fast reaction near the specimen edges was likely due to repeated breakdown of the scale during exposure. This paper will focus on the specimen centers; even then, scale thicknesses varied significantly, for example from 20 to 65 µm after 6.5 h exposure. As shown in the following, the reaction morphology evolved with exposure time. Due to the non-uniformity of the process, different reaction stages could be observed at different locations of a given specimen, with usually the more mature reaction morphologies located toward the specimen edges.

After 0.5 h reaction, the corrosion product consisted of a porous NiO scale. The sulfate above the scale was found to contain nickel to variable extents, corresponding to either solid or liquid Na_2SO_4–$NiSO_4$ solutions. In locations where the reaction was in its earliest stage, such as that shown in Fig. 4, nickel sulfide was found locally at the metal/oxide interface, wetting grain boundaries of both the nickel and the NiO. Analysis by SEM–EDS showed the sulfide to be Ni_3S_2 and to contain a small volume fraction of metallic Ni. This corresponds to the eutectic decomposition of the liquid Ni–S solution upon cooling to room temperature [8]. In these regions, the NiO was ∼2 µm thick and fully infiltrated with Na_2SO_4–$NiSO_4$. In other regions, nickel sulfide formed a continuous layer, the NiO was 5–10 µm thick and only its

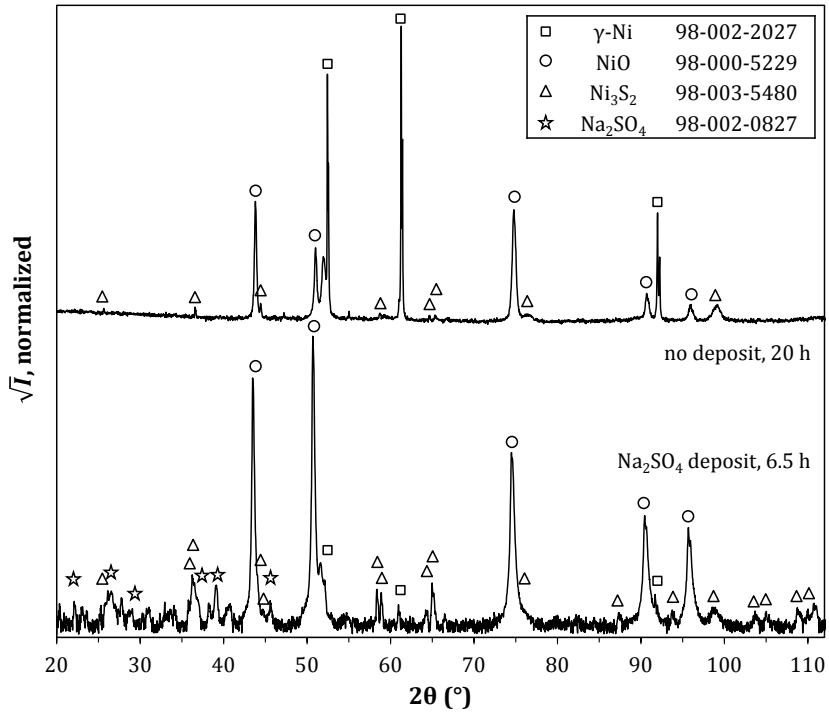

Figure 3: XRD analysis (Co radiation) of reaction products formed during exposure of nickel to O_2–0.1SO_2 at 700 °C, with and without Na_2SO_4 deposit.

outer half was permeated with the mixed sulfate.

Micrographs and WDS maps of the reaction product observed after 6.5 h reaction are shown in Fig. 5. The scale contains three distinct zones: an outer part of porous NiO infiltrated with Na_2SO_4–$NiSO_4$, an intermediate NiO layer with no sulfate, and a sulfide layer in contact with the metal. Examination of this specimen showed variations in the reaction morphology, which visibly represented successive stages of the same process. In Fig. 5a, the outer part of the scale has a complex, multi-layered microstructure, where a foam-like NiO network is embedded in a mixed sulfate (see insert). The intermediate, sulfate-free NiO layer displays an extensive, coarse porosity. Figure 5b shows a later stage: as the scale thickened, the intermediate layer constitutes an increasing proportion, it exhibits a finer porosity, and includes a significant fraction of Ni_3S_2. In places where the morphological evolution was visibly the most advanced, the scale consists of NiO with a fine, uniform porosity but no sulfate or sulfide, overlaying a sulfide layer. This morphology was observed along the entire specimen after 20 h. As shown in Fig. 6, in this later stage, the sulfur and sodium contents in the NiO layer showed local variations but remained small.

The presence of a significant fraction of nickel sulfide within the oxide layer, and its absence in a later stage, reflect important changes in the boundary conditions, which will be discussed in Section 4. Furthermore, the reaction products reflect both the reaction of NiO with the deposited sulfate, as is usually observed in hot corrosion, and a process of oxidation–sulfidation typical of exposures to SO_2-containing atmospheres. In order to evaluate the role of the Na_2SO_4 deposit and the gaseous

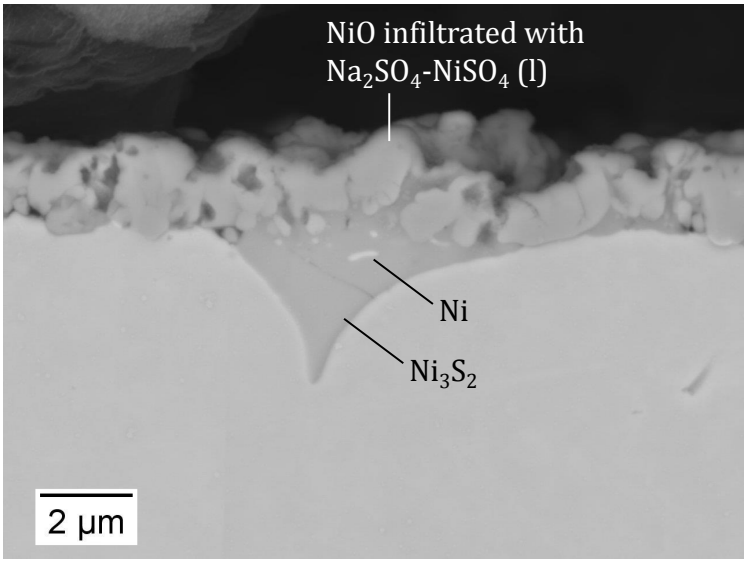

Figure 4: Corrosion product formed on nickel after 0.5 h reaction with Na_2SO_4 in O_2–$0.1SO_2$ at 700 °C. Observations with the salt retained showed that the NiO was infiltrated with Na_2SO_4–$NiSO_4$. This image was obtained after washing the sulfate off, and shows that NiO is also wetted with liquid sulfide.

sulfur in the reaction process, nickel specimens were exposed to Na_2SO_4 in dry air and to O_2–$0.1SO_2$ with no deposit, both for 20 h at 700 °C. A specimen was also reacted 20 h in dry air with no deposit to provide a baseline for nickel oxidation at this temperature. Micrographs of the reacted specimens are shown in Fig. 7, together with the specimen exposed 20 h to Na_2SO_4 in O_2–$0.1SO_2$.

The NiO scale grown in air with no deposit was 5 ± 1 µm thick, and displayed a cellular morphology typical of nickel oxidation at this temperature [23]. Reaction with Na_2SO_4 in air produced a porous, 15 ± 5 µm thick NiO scale, which contained a small amount of sulfur (1–2 at. %). Nickel sulfide was found locally below the NiO. It did not quite form a continuous layer, but wetted the nickel grain boundaries. The sulfate deposit was found to contain small amounts of nickel (< 2 at. %), which corresponds to sub-solidus compositions [10]. Its microstructure also indicated that it had remained solid. Exposure to O_2–$0.1SO_2$ with no deposit produced a similar reaction morphology. Qualitatively, the extent of sulfidation was smaller, but the NiO scale was thicker (30 ± 10 µm). Finally, the Na_2SO_4-coated specimen reacted in O_2–$0.1SO_2$ formed a 65 ± 10 µm NiO layer, with little sulfur and sodium, and a continuous layer of nickel sulfide. The latter penetrated the nickel grain boundaries down to several hundreds of microns. Figure 8 shows the Ni–Ni_3S_2 mixture formed after decomposition of the Ni–S liquid solution. The NiO layer is seen in Fig. 8 to be significantly porous — this was consistently observed throughout its entire thickness.

4 Discussion

The discussion will first consider the morphological evolutions observed during reaction of nickel with Na_2SO_4 in O_2–$0.1SO_2$, with a particular emphasis on the NiO

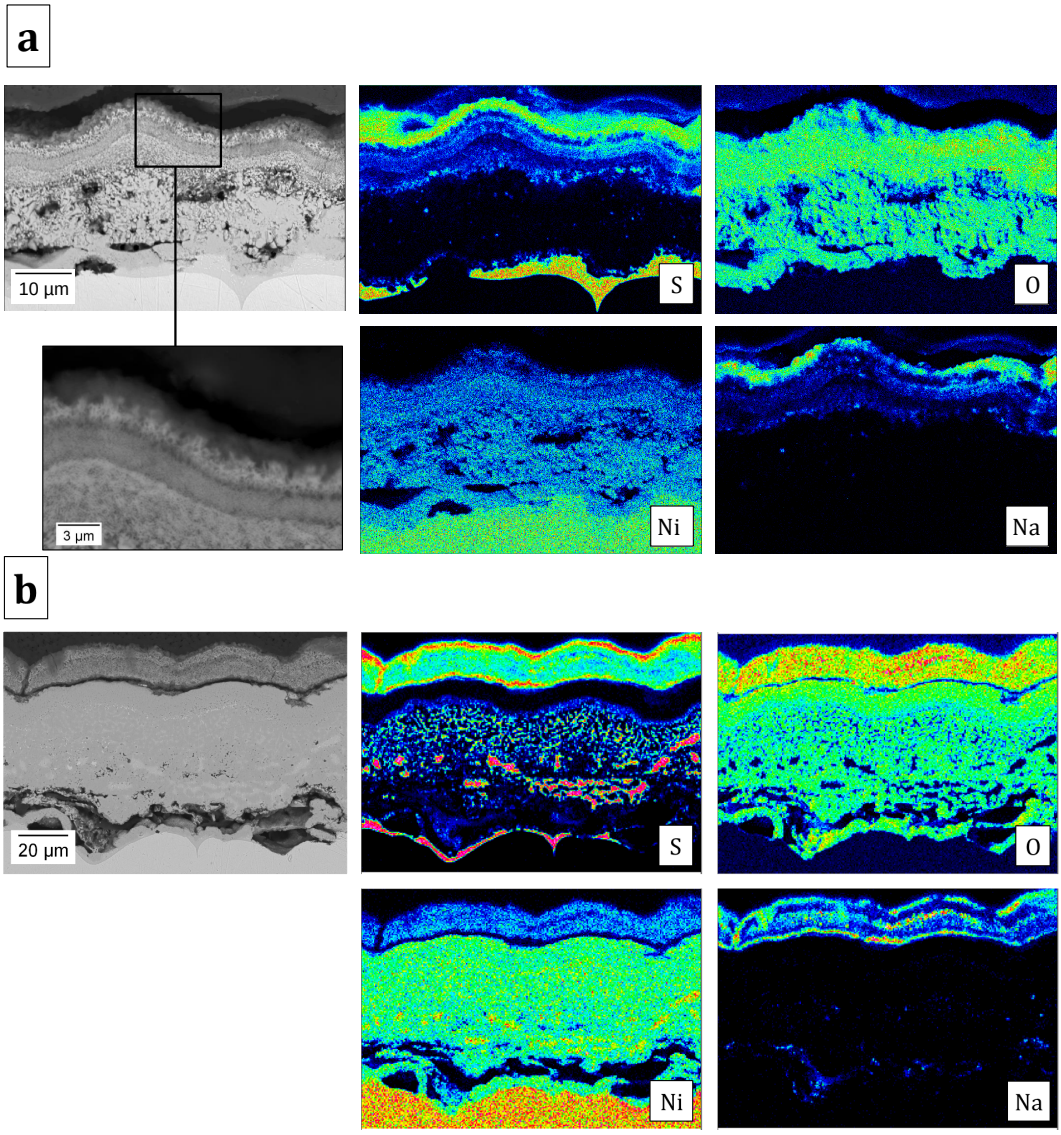

Figure 5: Back-scattered electron images and WDS maps of corrosion product formed after 6.5 h reaction of nickel with Na_2SO_4 in O_2–$0.1SO_2$ at 700 °C. The two regions come from the same specimen but reflect different stages of the reaction process: (a) in an earlier stage, the porous NiO scale is infiltrated with a Na_2SO_4–$NiSO_4$ solution in its top half (inset shows fine porosity in outer part); (b) in a later stage, the scale mostly contains a NiO + Ni_3S_2 mixture.

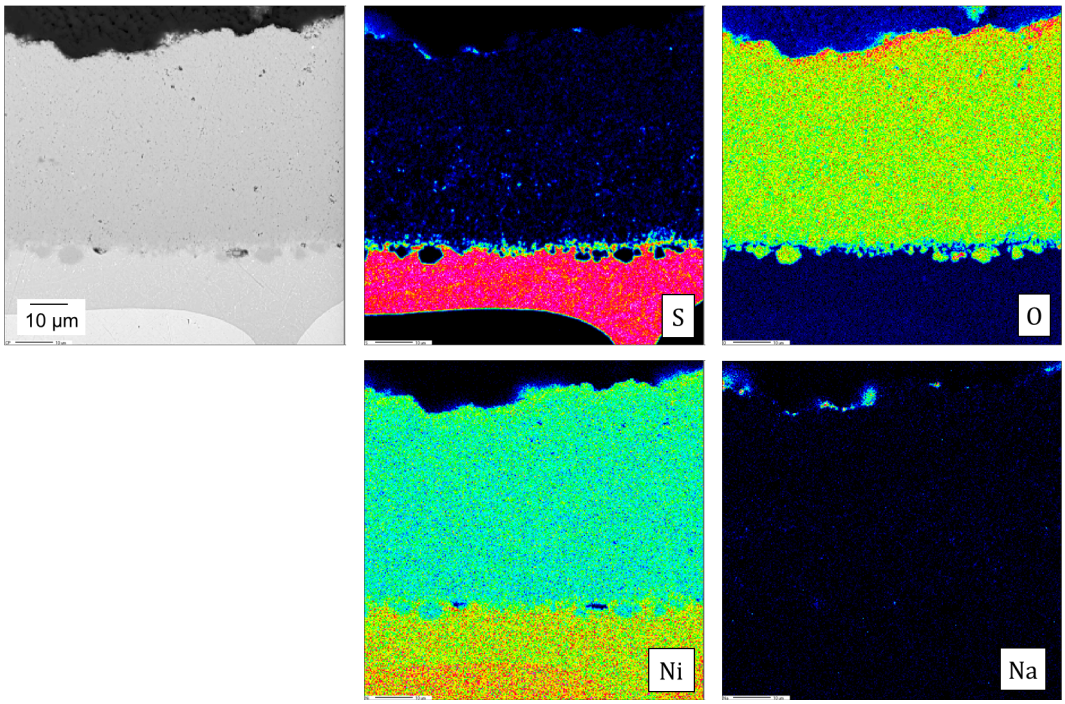

Figure 6: Back-scattered electron image and WDS maps of corrosion product formed after 20 h reaction of nickel with Na_2SO_4 in O_2–$0.1SO_2$ at 700 °C. The scale consists of a porous NiO layer, and a nickel sulfide layer in contact with the metal.

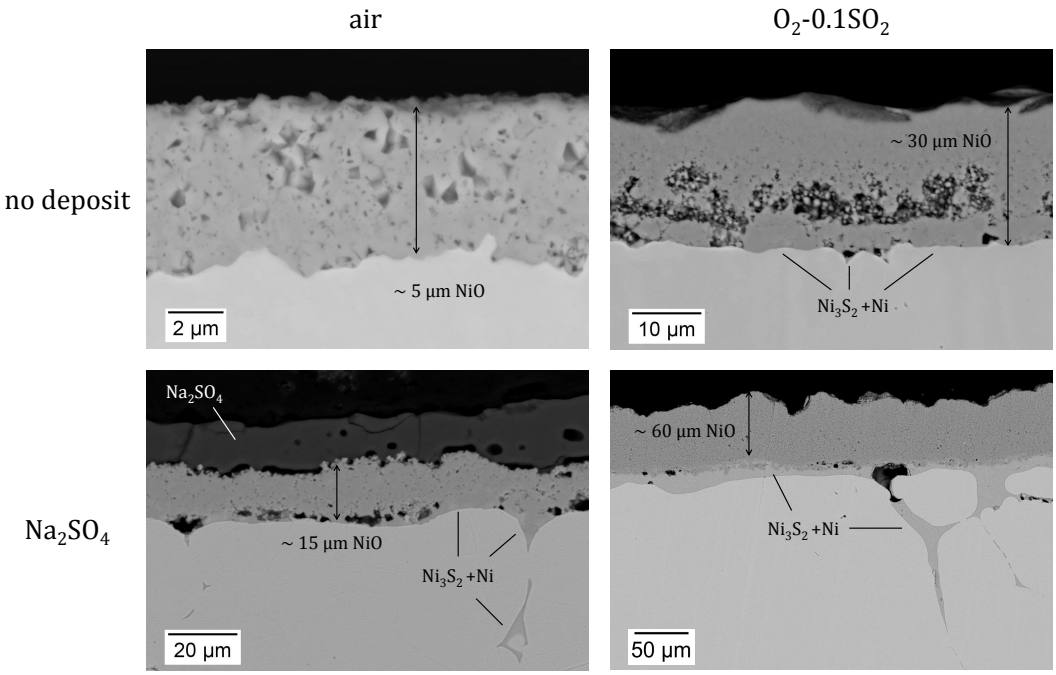

Figure 7: Corrosion product observed after 20 h reaction of nickel at 700 °C in air and O_2–$0.1SO_2$, with and without Na_2SO_4 deposit. The Ni–Ni_3S_2 mixture is formed upon cooling of liquid Ni–S.

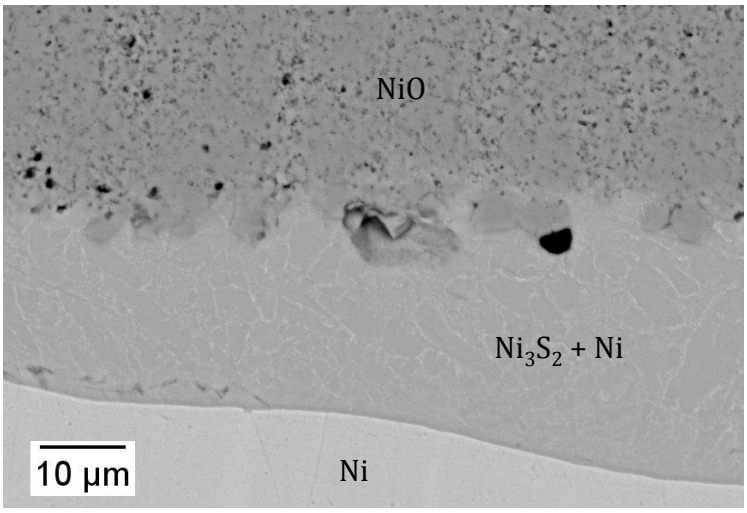

Figure 8: Detail of the Ni–Ni_3S_2 mixture and the porous NiO layer after 20 h reaction of nickel with Na_2SO_4 in O_2–0.1SO_2 at 700 °C.

dissolution process and in comparison with fluxing mechanisms known to occur at higher temperatures. We will then address the effect of the sulfate deposit on the oxidation–sulfidation process, in light of mechanisms prevailing in the absence of a deposit.

4.1 Mechanism of nickel reaction with Na_2SO_4

The stages of nickel reaction with Na_2SO_4 in O_2–0.1SO_2 at 700 °C are represented in Fig. 9 and can be summarized as follows. Oxidation first produces an NiO scale, which reacts with the sulfate to form a liquid Na_2SO_4–$NiSO_4$ solution. The melt then penetrates the porous NiO, eventually forming a layer of sulfate-infiltrated oxide in the outer part of the growing scale. Simultaneously, sulfidation occurs, first at the metal/oxide interface and in the inner part of the scale (Fig. 9a), then progressing until a significant fraction of the scale consists of nickel sulfide (Fig. 9b). In a later stage, the sulfate solution is no longer embedded in a distinct layer, but instead spread throughout the scale; sulfides are no longer present within the oxide, and sulfidation proceeds by thickening of a sulfide layer at the base of the scale (Fig. 9c).

This complex corrosion behavior can be analyzed in terms of two distinct yet interdependent processes: oxidation–sulfidation, which will be discussed subsequently, and the interaction between NiO and the sulfate in the outer part of the scale. The latter is addressed now, with an emphasis on the differences with type I hot corrosion.

In the early stage of the reaction, NiO dissolves into an initially nickel-free sulfate, i.e., along a negative concentration gradient. However, SO_3 consumption to form $NiSO_4$ results in a local p_{SO_3} decrease at the oxide/sulfate interface, and, since the Ni^{2+} solubility is an increasing function of p_{SO_3}, this produces a positive solubility gradient, as represented in Fig. 10. The opposed concentration and solubility gradients lead to rapid saturation of the melt with Ni^{2+}. Furthermore, the continued consumption of oxygen and sulfur (associated with the oxidation–sulfidation of

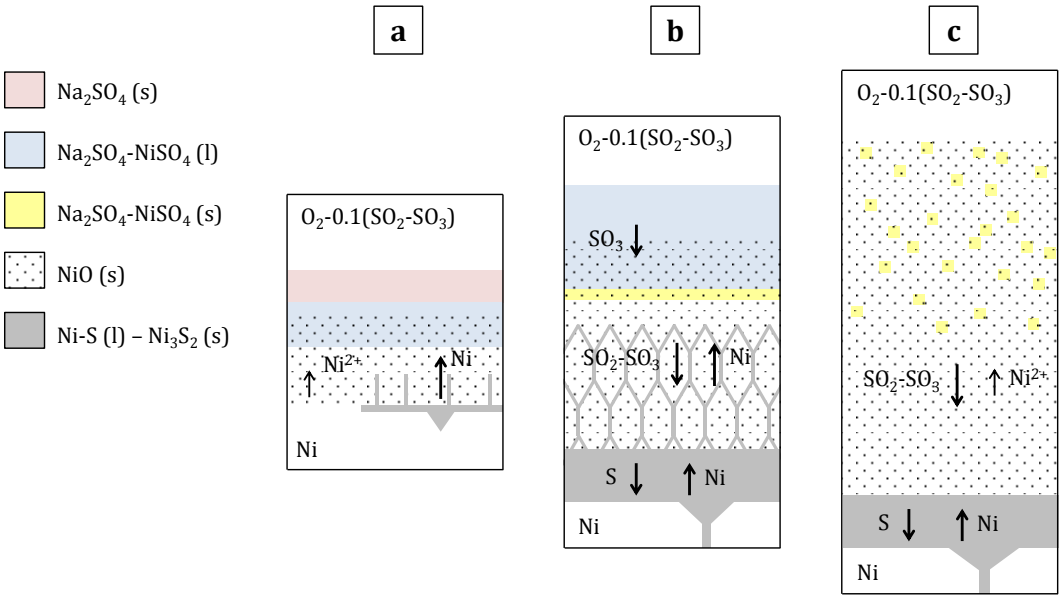

Figure 9: Schematic representation of microstructural evolution and transport processes during reaction of nickel with Na_2SO_4 in O_2–0.1SO_2 at 700 °C. Successive steps represent: (a) NiO dissolution in Na_2SO_4 and infiltration of the mixed sulfate in the oxide layer; (b) sulfide development within the oxide layer; (c) growth of porous NiO (details given in text).

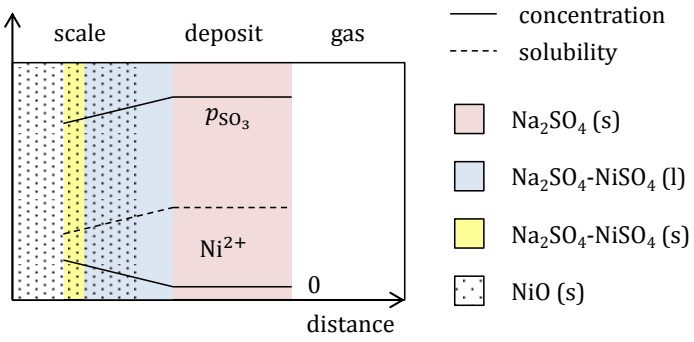

Figure 10: Schematic representation of the activity gradients in the early stage of NiO dissolution in Na_2SO_4, during reaction of nickel with Na_2SO_4 in O_2–0.1SO_2 at 700 °C.

the nickel) maintains a reduced p_{SO_3}, which favors the precipitation of NiO at the oxide/sulfate interface. This results in the foam-like oxide microstructure observed in the outer part of the scale (see insert in Fig. 5a). Indeed, as noted by Misra and Whittle [24], if the p_{SO_3} at the oxide/sulfate interface decreases below a certain value, the liquid solution is no longer stable, and dissociates into NiO and a solid Na_2SO_4–$NiSO_4$ solution. In the present situation where the gas p_{SO_3} is only slightly higher than the threshold value (Fig. 1), this is expected to occur. The precipitation explains why the sulfate solution is confined to an outer region of the scale, and does not infiltrate the oxide to a deeper level.

Thus, during the course of the corrosion process, the system chemistry evolves to allow the acidic dissolution of NiO, and its precipitation. Yet these occur as successive events at the same interface (oxide/sulfate): after the sulfate is saturated

with Ni^{2+} due to the decrease in p_{SO_3}, the conditions for NiO dissolution are no longer met, and the reverse process, precipitation, occurs instead. This is an essential difference with type I conditions, where basic dissolution and precipitation occur simultaneously at two different interfaces (oxide/sulfate and sulfate/gas, respectively), and both can be sustained for some time (before eventually stopping, see details in Ref. [1]). Specifically, no negative solubility gradient can be established during type II hot corrosion of a pure metal with a pure Na_2SO_4 deposit. Indeed, at temperatures below the melting point of Na_2SO_4, the formation of a liquid requires the acidic dissolution of the metal oxide, which involves a relatively acidic atmosphere. Thus the direction of the p_{SO_3} gradient imposes a positive solubility gradient for acidic solutes. Several authors [4, 12] anticipated that in these conditions, and in the absence of an M^{2+}–M^{3+} exchange mechanism for nickel, no accelerated corrosion would take place.

This prediction is verified here to some extent, since no continued dissolution-precipitation occurs, and the corrosion product does not present the layered morphology typical of type I conditions. In the longer term, oxidation causes the nickel-saturated Na_2SO_4–$NiSO_4$ solution to be embedded in an increasing volume of oxide, until it no longer forms an interconnected phase but is dispersed throughout the scale. So long as no fresh Na_2SO_4 is provided, the reaction is limited to an oxidation–sulfidation process. However, while it is interconnected, the sulfate solution does have an influence on the extent of oxidation and sulfidation; this will be discussed now.

4.2 Mechanism of the oxidation–sulfidation process

From a simple gas-phase thermodynamics perspective, sulfidation is not expected to occur in O_2–$0.1SO_2$ at 700 °C, since the equilibrium gas composition is oxidizing but non-sulfidizing to nickel (Fig. 1). However, as proposed by Goebel and Pettit [1], in the presence of a sulfate deposit, oxygen consumption to form NiO may lead to an elevated sulfur activity at the oxide/sulfate interface, by virtue of Eq. (1). Even in the absence of a deposit, sulfidation may occur if the oxide is permeable to sulfur-bearing molecules, and the SO_2 pressure is high enough for the p_{S_2} to exceed the sulfide dissociation pressure at the low p_{O_2} prevailing within the scale, as discussed by Birks et al. [25, 26]. This requires the oxide defects to be sufficiently small for the molecular species they contain to be in (or tend to) local equilibrium with the surrounding oxide, such that activity gradients develop. Sulfides may then form within the oxide or at the metal/oxide interface, where the p_{O_2} is minimum and the p_{S_2} maximum.

Here both the presence of a sulfate deposit and local equilibrium within the oxide scale contribute to the establishment of sulfidizing conditions. The constitution of the reaction products indicates that a moderately high sulfur activity was reached initially. At 700 °C, the sequence of phases in the Ni–S system is [8]: Ni, Ni–S (l), Ni_3S_2, $Ni_{1-x}S$, NiS_2, S_2 (g); yet $Ni_{1-x}S$ and NiS_2 were not observed. Sulfidation is seen to occur first atop nickel grain boundaries (Fig. 4); preferential nucleation at the triple junction reflects a limited sulfur supersaturation, which favors the lower sulfides. (In addition, once the liquid sulfide is formed, fast diffusion maintains a nickel activity close to unity at its surface, thus destabilizing the higher sulfides). As the reaction proceeds, however, a continuous Ni–S (l) layer is established at the

metal/oxide interface, and Ni_3S_2 is eventually formed throughout the scale (Fig. 5b). The requisite increase in p_{S_2} for this to occur is related to the deposit. Specifically, in the outer part of the scale, the sulfate forms an interconnected solution, effectively sealing the scale and allowing the p_{O_2} to further decrease and the p_{S_2} to further increase. Eventually, as the sulfate is dispersed throughout the growing scale, the p_{S_2} is reduced and Ni_3S_2 is no longer stable within the scale. Local equilibrium between SO_2–SO_3 and NiO still maintains sulfide stability at the metal/oxide interface.

The discussion now turns to the question of sulfur transport through the NiO. As noted in the Introduction, mixed NiO–Ni_3S_2 scales formed during gaseous oxidation–sulfidation of nickel in high SO_2/O_2 environments can grow as much as seven orders of magnitude faster than NiO would, due to the fast diffusion of nickel in the sulfide. In the present case, the Ni_3S_2 present within the NiO was, at some stage of the process, interconnected (see Fig. 5b), and presumably sustained such a rapid reaction for a period. Yet the sulfides eventually dissociated, and scale growth must then have relied on another transport mechanism. Measuring reaction kinetics proved difficult because of the non-uniformity of the scale and the succession of different reaction regimes. On the basis of scale thickness measurements, the reaction rate is qualitatively seen to decrease with time. Assuming parabolic kinetics for comparison purposes, a k_p is estimated to be 10^{-9} cm^2 s^{-1}, while that of sulfidation is reported to be about 10^{-6} cm^2 s^{-1} at 700 °C [18], three orders of magnitude higher. On the other hand, the estimated k_p far exceeds that of NiO growth, about 10^{-13} cm^2 s^{-1}, which at this temperature is supported by short-circuit nickel diffusion [19]. Thus, the observed scaling is too fast to be sustained by solid-state diffusion. Since the scale is extensively porous (see Fig. 8), inward molecular oxygen transport is a more likely candidate.

The diffusivity of sulfur in NiO at 700 °C is not known, and extrapolation to 700 °C of measurements made at higher temperatures using single crystals would be unreliable, since grain boundary diffusion predominates at lower temperatures. Reviewing the limited solubility and diffusivity data available, several authors [6,27] have argued that the continued growth of a sulfide layer below the oxide scale in situations of oxidation–sulfidation must involve transport of sulfur-bearing molecules across the scale. It is concluded that in the present case, molecular transport via SO_2–SO_3 allowed the rapid supply of both oxygen and sulfur across the porous NiO layer. The relative amounts of SO_2 and SO_3 depend on the local thermodynamic conditions. Even though the NiO layer is porous, local equilibrium imposes a p_{O_2} gradient, such that the equilibrium SO_2/SO_3 ratio increases toward the sulfide/oxide interface. Using the equilibrium constant for reaction (6) at 700 °C calculated from data in Ref. [7], limiting values of this ratio are found to be 4×10^{-1} for $p_{O_2} = 1$ atm and 5×10^{7} at the NiO dissociation pressure on Ni, $p_{O_2} = 5 \times 10^{-17}$ atm. Whether SO_2 actually predominates within the scale depends on the ability of NiO to catalyze reaction (6); if the reaction is sluggish, the gas mixture might become supersaturated with SO_3 at low p_{O_2} values.

The liquid Ni–S is likely a fast diffuser of both nickel and sulfur. As a consequence, sulfide growth may occur together with NiO at the sulfide/oxide interface

$$7Ni + 2SO_2 = 4NiO + Ni_3S_2 \tag{8}$$

and at the metal/sulfide interface by sulfur diffusion inward. In the latter case NiO

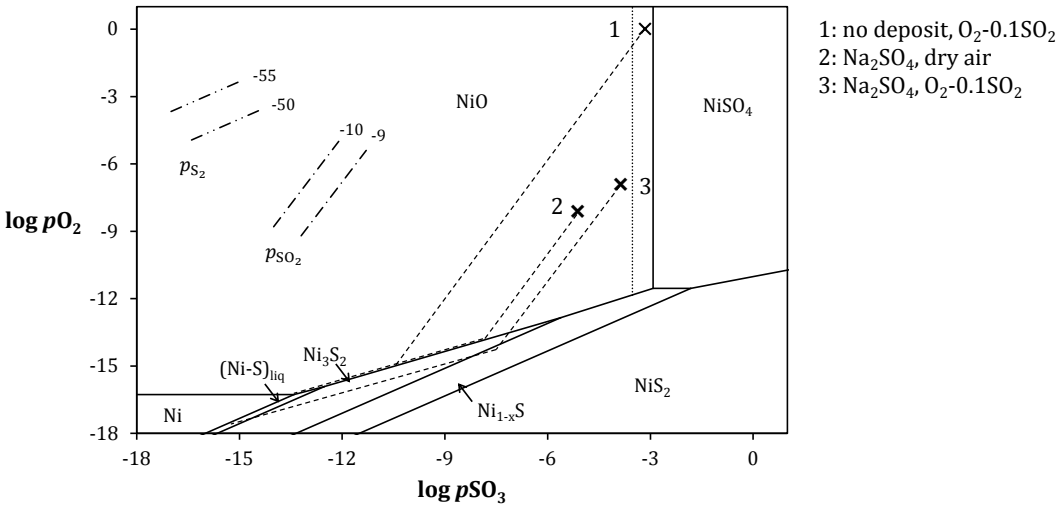

Figure 11: Tentative reaction paths for the reaction of nickel with Na_2SO_4 in O_2–$0.1SO_2$, with no deposit in O_2–$0.1SO_2$, and with Na_2SO_4 in dry air. The crosses mark the thermodynamic conditions estimated at the scale surface for each environment (see text).

is formed at the expense of the sulfide by the displacement reaction:

$$Ni_3S_2 + \frac{3}{2}SO_2 = 3NiO + \frac{7}{4}S_2 \tag{9}$$

(the sulfide is assumed to have the stoichiometry of Ni_3S_2 for simplification). Of course, as noted earlier, the formation of a sulfide layer implies that it is more stable than the oxide at the metal surface; however, the activity gradients across the scale cause reaction (8) to proceed to the right at the sulfide/oxide interface. Whether the net result at the sulfide/oxide interface is growth or consumption of the sulfide depends on the relative rates of mass transport and of reactions (8) and (9) — this question has been discussed in detail by previous investigators [6, 15, 16, 27]. The mass transport processes discussed here are summarized in Fig. 9. In the later stage of the reaction, although NiO is, intrinsically, a cation diffuser, oxide growth occurs predominantly at the sulfide/oxide interface because inward molecular oxygen transport is faster than the outward ionic diffusion of nickel.

4.3 Role of the environment in the oxidation–sulfidation process

As discussed above, the presence of an interconnected sulfate solution in the scale has an influence on the boundary conditions governing the oxidation–sulfidation process. This in turn affects the constitution and growth rate of the corrosion product. A similar observation is arrived at when comparing the results of the "Na_2SO_4/O_2–$0.1SO_2$", "no deposit/O_2–$0.1SO_2$" and "Na_2SO_4/dry air" experiments (Fig. 7). The roles of the sulfate deposit and gas atmosphere are now examined further. To do so, reaction paths for the three experiments are constructed by reporting the activities prevailing at the metal/scale and scale/gas (or scale/deposit) interfaces on the stability diagram of Fig. 11.

The thermodynamic conditions at the scale/gas interface during the "no deposit/O_2–$0.1SO_2$" experiment are simply defined by the equilibrium gas composition; these

are marked as point 1 in Fig. 11. In the "Na_2SO_4/dry air" experiment, sulfur could only be obtained from dissociation of the sulfate. The absence of a significant p_{SO_3} in the flowing gas has two implications: no liquid Na_2SO_4–$NiSO_4$ solution can be stabilized, and gas–solid equilibrium indeed requires that reaction (3) proceeds to the right, i.e., that the sulfate releases some SO_3. Incidentally, SO_3 removal from the sulfate further precludes any liquid formation as it reduces Ni^{2+} solubility; indeed, the deposit appeared to have remained solid, and it was found by SEM–EDS to contain only traces of nickel, corresponding to a solid Na_2SO_4–$NiSO_4$ solution. Despite remaining solid, the deposit must have effectively sealed the oxide in order for sulfidizing conditions to develop. Based on these observations, it is concluded that the p_{O_2} and the p_{SO_3} at the oxide/sulfate interface were lower than in the O_2–$0.1SO_2$ atmosphere; estimated values are indicated as point 2 in Fig. 11. In the "Na_2SO_4/O_2–$0.1SO_2$" experiment, again boundary conditions are estimated relative to those prevailing in the two other experiments. As discussed in Section 4.1, oxidation and sulfidation of the nickel produced activity gradients across the sulfate, resulting in both p_{SO_3} and p_{O_2} lower below the sulfate than in the flowing gas. The infiltrated sulfate was saturated with nickel, so the p_{SO_3} at the oxide/sulfate interface was most likely higher than in the "Na_2SO_4/dry air" experiment, where Na_2SO_4 contained only traces of nickel. The p_{O_2} also was presumably higher, since mass transport would have been faster in a partially molten sulfate than in a solid form. An estimated gas composition is shown as point 3 in Fig. 11.

We now turn to the conditions prevailing at the metal/scale interface. In the "no deposit/O_2–$0.1SO_2$" experiment, sulfidation was localized and limited in extent, which suggests that the sulfur supersaturation with respect to Ni (s) was small, i.e., that the (p_{O_2}, p_{SO_3}) couple was relatively close to the Ni/NiO/Ni–S (l) triple point. In the "Na_2SO_4/dry air" experiment, sulfidation was also local but occurred to a greater extent; finally, in the "Na_2SO_4/O_2–$0.1SO_2$" experiment, the continuous sulfide layer indicates that the reaction path crossed the NiO/Ni–S (l) phase boundary.

Based on these observations, tentative reaction paths are plotted in Fig. 11 for the three experiments. The orientation of these paths depends on the way the gas composition evolves across the porous NiO layer. Since the oxide scales formed in the three situations present similar microstructures, the paths are plotted parallel to one another. This graphical construction shows that the experimental results are consistent with an evolution of the gas composition following SO_2 isobars, rather than SO_3 isobars. We conclude that in O_2–$0.1SO_2$, the main influence of adding a sulfate deposit is to lower both p_{SO_3} and p_{O_2} at the oxide surface, in a ratio which generates an increased sulfur activity and eventually leads to enhanced sulfidation. When a deposit is present, adding SO_2–SO_3 to the gas leads to an increased p_{SO_3} below the deposit, which also favors sulfidation. Another effect of the presence of sulfur is the formation of a porous NiO; this is discussed next.

4.4 Role of sulfur in the NiO microstructures

All three corrosion tests involving sulfur, in the form of Na_2SO_4 deposits, O_2–$0.1SO_2$ gas or both, resulted in the fast growth (i.e., faster than in air) of porous NiO scales. It is noted that the NiO scale grown in air also presented some, much smaller, degree of porosity (Fig. 7). Scales grown in air or oxygen at temperatures lower than 1000 °C usually consist of two layers, with the porous inner layer growing by

inward oxygen transport [23]. In the extensive study of nickel oxidation in oxygen by Peraldi et al. [23], scales grown at 700 °C were described to present an extensive open porosity. Yet, even though oxidation involved molecular oxygen transport inward, oxidation kinetics were controlled by solid-state nickel diffusion, along short-circuits (e.g., grain boundaries, dislocations pipes or pore surfaces) at this relatively low temperature. This is also the case in the present study, where the measured oxide thickness after reaction in air with no deposit, 5 ± 1 µm, is consistent with reported growth rates based on short-circuit nickel diffusion [19]. As is evident in Figs. 7 and 8, both the porosity and the growth rate of the NiO scales formed in the presence of sulfur were significantly greater. As discussed earlier, this fast growth is due to inward transport of SO_2–SO_3, which also provided the sulfur for sulfidation.

A question of interest, then, is how the presence of sulfur in the system led to an extensively porous microstructure. Goebel and Pettit [1] argued that porous NiO scales could be obtained by oxidation of nickel sulfide: for a sufficiently high sulfur activity in the sulfide, p_{SO_2} at the sulfide/oxide interface would exceed 1 atm, such that gas evolution would mechanically rupture the oxide and yield a porous scale. A comparison of the tests conducted here with Na_2SO_4 or O_2–$0.1SO_2$ in Fig. 7 shows that the oxide scales formed in these conditions all had a similar microstructure, including similar degrees of porosity, despite the sulfide being only present locally in the "no deposit/O_2–$0.1SO_2$" and "Na_2SO_4/dry air" experiments. Thus the porosity in this case was not specifically due to the displacement reaction, and must have involved sulfur in some other way. Smialek [28] reported the fast growth of porous Al_2O_3 on highly S- and Zr-doped NiAl in air at 1200 °C. The NiAl/Al_2O_3 and Ni/NiO systems are obviously very different, but Smialek argued that an open network of submicron microchannels served as paths for rapid gas transport, and also concluded that the widespread porosity was due to SO_2 evolution. A similar mechanism might be operating here. Alternatively, or in addition, sulfur is known to segregate at metal/oxide interfaces, where it is thought to stabilize interfacial pores by reducing their surface energy, which can have the effect of lessening the oxide adherence [29]. Preferential sulfur adsorption at pore surfaces may also hinder kinetic processes to the extent that a porous NiO scale results, although this remains to be investigated in more detail.

5 Conclusions

The reaction of nickel with Na_2SO_4 in O_2–$0.1SO_2$ at 700 °C was analyzed in terms of two processes: (1) the interaction between the thermally grown NiO scale and the sulfate deposit; and (2) the simultaneous oxidation–sulfidation of the nickel. The acidic dissolution of NiO in the Na_2SO_4 produced a liquid sulfate solution, which infiltrated the porous oxide. In the absence of a negative solubility gradient, the liquid sulfate was rapidly saturated with nickel. Eventually, oxygen and sulfur consumption led to the precipitation of NiO and a solid sulfate solution, which dispersed throughout the growing scale. The reaction was then reduced to an oxidation–sulfidation process.

Sulfidation was also found to occur with no deposit in O_2–$0.1SO_2$, and with Na_2SO_4 in air. The role of the deposit and atmosphere on the boundary conditions relative to the oxidation–sulfidation process was studied by analyzing the reaction

path associated with each environment. In O_2–$0.1SO_2$, adding Na_2SO_4 led to lower p_{O_2} and p_{SO_3} levels at the oxide surface due to slow mass transport, in a ratio which corresponded to an increased sulfur activity, which led to enhanced sulfidation. When a deposit was present, adding SO_2–SO_3 to the gas led to a greater sulfur activity at the oxide/sulfate interface, and also promoted sulfidation.

Finally, although NiO scales grown in air with no sulfate deposit tend to develop some degree of porosity, the extent is much greater in the presence of sulfur, whether added as Na_2SO_4 or as SO_2–SO_3 (g). This phenomenon may be associated with the tendency of sulfur to preferentially adsorb on internal surfaces and poison reaction processes (e.g., oxidation and sintering).

Acknowledgements

This work was supported by the Department of Energy through the University Turbine Systems Research Program run by the National Energy Technology Laboratory, award number DE–FE0007271, Dr. Seth Lawson, project manager. The authors thank Prof. G.H. Meier at the University of Pittsburgh for useful discussions, as well as the reviewers for useful suggestions.

References

[1] J. A. Goebel and F. S. Pettit, Na_2SO_4-induced accelerated oxidation (hot corrosion) of nickel, Metallurgical Transactions 1 (1970) pp. 1943–1954. doi: 10.1007/BF02642794.

[2] R. Rapp and K. Goto, in *Second International Symposium on Molten Salts* (J. Braunstein and J. Selman, eds.) The Electrochemical Society, Pennington (1981).

[3] R. A. Rapp, Chemistry and electrochemistry of the hot corrosion of metals, Corrosion 42 (1986) pp. 568–577. doi: 10.5006/1.3583026.

[4] N. Otsuka and R. Rapp, Hot corrosion of preoxidized Ni by a thin fused Na_2SO_4 film at 900 °C, Journal of the Electrochemical Society 137 (1990) pp. 46–52. doi: 10.1149/1.2086436.

[5] K. L. Luthra and D. A. Shores, Mechanism of Na_2SO_4 induced corrosion at 600 °C–900 °C, Journal of the Electrochemical Society 127 (1980) pp. 2202–2210. doi: 10.1149/1.2129375.

[6] N. Birks, G. H. Meier and F. S. Pettit, *Introduction to the High Temperature Oxidation of Metals*. Cambridge University Press 2nd ed. (2006).

[7] I. Barin, *Thermochemical Data of Pure Substances*. VCH second ed. (1993).

[8] P. Waldner and A. D. Pelton, Thermodynamic modeling of the Ni–S system, Zeitschrift für Metallkunde 95 (2004) pp. 672–681. doi: 10.3139/146.018005.

[9] A. K. Misra, D. P. Whittle and W. L. Worrell, Thermodynamics of molten sulfate mixtures, Journal of the Electrochemical Society 129 (1982) pp. 1840–1845. doi: 10.1149/1.2124305.

[10] H. M. E.M. Levin and M. Reser, *Phase Diagrams for Ceramists 1975 supplement*. The American Ceramic Society, Westerville (1975).

[11] K. L. Luthra, Low-temperature hot corrosion of cobalt-base alloys. 1. Morphology of the reaction product, Metallurgical Transactions A 13 (1982) pp. 1843–1852. doi: 10.1007/bf02647841.

[12] K. L. Luthra, Low-temperature hot corrosion of cobalt-base alloys. 2. Reaction mechanism, Metallurgical Transactions A 13 (1982) pp. 1853–1864. doi: 10.1007/bf02647842.

[13] K. Lillerud and P. Kofstad, Sulfate-induced hot corrosion of nickel, Oxidation of Metals 21 (1984) pp. 233–270. doi: 10.1007/BF00656835.

[14] M. F. Stroosnijder and W. J. Quadakkers, Review of high temperature corrosion of metals and alloys in sulphidizing/oxidizing environments. I. Corrosion of metals, High Temperature Technology 4 (1986) pp. 83–96. doi: 10.1080/02619180.1986.11753321.

[15] P. Kofstad, *High temperature corrosion.* Elsevier Applied Science Publishers (1988).

[16] F. Gesmundo, D. J. Young and S. Roy, The high temperature corrosion of metals in sulfidizing-oxidizing environments: a critical review, High Temperature Materials and Processes 8 (1989) pp. 149–190. doi: 10.1515/HTMP.1989.8.3.149.

[17] K. L. Luthra and W. L. Worrell, Simultaneous sulfidation-oxidation of nickel at 603 °C in argon–SO_2 atmospheres, Metallurgical Transactions A 9 (1978) pp. 1055–1061. doi: 10.1007/BF02652209.

[18] S. Mrowec and K. Przybylski, Transport properties of sulfide scales and sulfidation of metals and alloys, Oxidation of Metals 23 (1985) pp. 107–139. doi: 10.1007/BF00659899.

[19] R. Peraldi, D. Monceau and B. Pieraggi, Correlations between growth kinetics and microstructure for scales formed by high-temperature oxidation of pure nickel. II. Growth kinetics, Oxidation of Metals 58 (2002) pp. 275–295. doi: 10.1023/A:1020102604090.

[20] K. L. Luthra and W. L. Worrell, Simultaneous sulfidation-oxidation of nickel at 603 °C in SO_2–O_2–SO_3 atmospheres, Metallurgical Transactions A 10 (1979) pp. 621–631. doi: 10.1007/BF02658326.

[21] C. S. Giggins and F. S. Pettit, Corrosion of metals and alloys in mixed gas environments at elevated temperatures, Oxidation of Metals 14 (1980) pp. 363–413. doi: 10.1007/BF00603609.

[22] T. Gheno, M. Zahiri Azar, A. Heuer and B. Gleeson, Reaction morphologies developed by nickel aluminides in type II hot corrosion conditions: the effect of chromium, Corrosion Science 101 (2015) pp. 32–46. doi: 10.1016/j.corsci.2015.08.029.

[23] R. Peraldi, D. Monceau and B. Pieraggi, Correlations between growth kinetics and microstructure for scales formed by high-temperature oxidation of pure nickel. I. Morphologies and microstructures, Oxidation of Metals 58 (2002) pp. 249–273. doi: 10.1023/A:1020170320020.

[24] A. K. Misra and D. P. Whittle, Effects of SO_2 and SO_3 on the Na_2SO_4 induced corrosion of nickel, Oxidation of Metals 22 (1984) pp. 1–33. doi: 10.1007/bf00659246.

[25] N. Birks, Corrosion mechanisms of metals and alloys in multicomponent oxidative environments, in *Proceedings of the symposium on properties of high temperature alloys with emphasis on environmental effects (Electrochemical Society, Las Vegas, 1976)* (Z. Foroulis and F. Pettit, eds.) p. 215.

[26] M. C. Pope and N. Birks, The penetration by sulfur of NiO scales growing on nickel, Oxidation of Metals 12 (1978) pp. 173–181. doi: 10.1007/BF00740258.

[27] D. J. Young, *High Temperature Oxidation and Corrosion of Metals*. Elsevier Corrosion Series Elsevier (2008).

[28] J. L. Smialek, Non-protective alumina growth in sulfur-doped NiAl(Zr), Materials at High Temperatures 17 (2000) pp. 71–77. doi: 10.1179/mht.2000.012.

[29] T. Gheno, D. Monceau, D. Oquab and Y. Cadoret, Characterization of sulfur distribution in Ni-based superalloy and thermal barrier coatings after high temperature oxidation: a SIMS analysis, Oxidation of Metals 73 (2010) pp. 95–113. doi: 10.1007/s11085-009-9164-z.